*Australian Meteorological and Oceanographic Journal 64* (2014) 345–356

# Seasonal climate summary southern hemisphere (autumn 2014): tropical Pacific experiences strong push toward El Niño

**Catherine Ganter**
Climate Monitoring and Prediction, Bureau of Meteorology, Australia

(Manuscript received March 2015; revised March 2015)

Southern hemisphere circulation patterns and associated anomalies for the austral autumn 2014 are reviewed, with emphasis given to the Pacific Basic climate indicators and Australian rainfall and temperature patterns. The tropical Pacific saw a number of indicators make a strong push toward El Niño during the autumn months. In the eastern tropical Pacific, warm sea surface temperature anomalies emerged during autumn, while in March the Southern Oscillation Index (SOI) saw its most negative monthly value since February 2010 (the end of the last El Niño), with –13.3. Outside the tropics, the Southern Annular Mode (SAM) was slightly positive, but within the neutral range during autumn. For the Australian region, sea surface temperatures ranked as fourth warmest on record. The Australian area-averaged land surface maximum temperature anomaly was +1.16 °C for autumn, sixth-warmest on record. Similarly, minimum temperatures were also above average (+1.14 °C) and third-warmest on record. Spatially, both maximum and minimum temperatures showed a virtual absence of below average temperatures for autumn across Australia. Rainfall was nine per cent below average for Australia, with a wetter than average autumn for much of the south to southeast, and a drier than average autumn for southwest Queensland and parts of northwest Western Australia.

## Introduction

This summary reviews the southern hemisphere and equatorial climate patterns for autumn 2014, with particular attention given to the Australasian and Pacific regions. The main sources of information for this report are analyses prepared by the Bureau of Meteorology.

## Pacific and Indian Basin climate indices

### Southern Oscillation Index

The Troup Southern Oscillation Index[1] (SOI) for the period January 2010 to May 2014 is shown in Fig. 1, together with a five-month weighted moving average. Persistent values of the SOI can reflect El Niño–Southern Oscillation (ENSO) events. For example, the La Niña conditions of 2010 and 2011 can be seen clearly in the SOI as a sustained period of strongly positive values.

2013 was an ENSO-neutral year, with no sustained deviation in SOI values. 2014 began with a relatively strong positive value in January (+12.2), with March showing a strong swing into negative territory (–13.3), coinciding with a swing in other indicators of El Niño. This was the strongest negative monthly value since February 2010, the end of the last El Niño. However, the other autumn months, April and May, saw a return to positive values (+8.6 and +4.4, respectively), with the average autumn SOI –0.1. The autumn mean sea level pressure (MSLP) values for Darwin were 0.5 hPa above average at 1009.9 hPa and 0.2 hPa above average for Tahiti with 1012.3 hPa. The monthly anomalies for Darwin in March, April and May 2014 were +1.5, –0.6 and +0.7 hPa respectively, and for Tahiti, –1.0, +0.4 and +1.3 hPa respectively. The overall positive MSLP anomaly at Darwin is consistent with a drier than usual autumn for the region (see rainfall section).

[1]The Troup Southern Oscillation Index (Troup 1965) used in this article is ten times the standardised monthly anomaly of the difference in mean sea level pressure (MSLP) between Tahiti and Darwin. The calculation is based on a sixty-year climatology (1933–1992). The Darwin MSLP is provided by the Bureau of Meteorology, with the Tahiti MSLP provided by Météo France inter-regional direction for French Polynesia.

*Corresponding author address:* Catherine Ganter, Bureau of Meteorology, Melbourne. Email: c.ganter@bom.gov.au.

Fig. 1. Southern Oscillation Index (SOI), from January 2010 to May 2014, together with a five-month binomially weighted moving average. The means and standard deviations used in the computation of the SOI are based on the period 1933–1992.

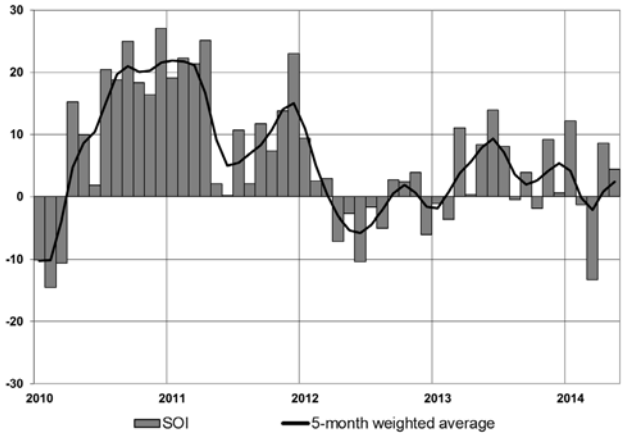


Fig. 2. 5VAR composite standardised monthly ENSO index from January 2010 to May 2014, together with a weighted three-month moving average. See text for details.

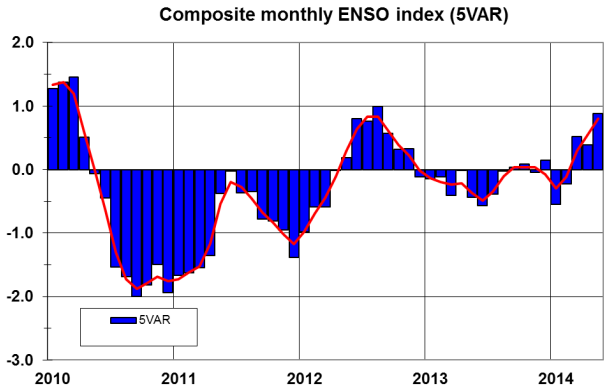


### Composite monthly ENSO index (5VAR) // MEI

5VAR[2] is a composite monthly ENSO index, calculated as the standardised amplitude of the first principal component of monthly Darwin and Tahiti MSLP[3] and monthly NINO3, NINO3.4 and NINO4 sea-surface temperatures[4] (SSTs). The monthly 5VAR values for the period January 2010 to May 2014 are shown in Fig. 2, along with the weighted three-month moving average. Persistently positive (negative) values in excess of one standard deviation indicate El Niño (La Niña).

The rapid end of the 2009–10 El Niño in autumn 2010 can be seen in Fig. 2 (Campbell 2011), as can the fast development of the 2010–11 La Niña (Ganter 2011) occurring later that year, with a lull during winter 2011 (Tobin 2012). La Niña redevelopment occurred in spring 2011 (Cottrill 2012). Conditions came close to El Niño in winter 2012 (Pepler 2013), but otherwise conditions have been ENSO-neutral since late 2012. 2014 saw increasingly positive values of the 5VAR index, with values for March, April and May measuring +0.52, +0.39 and +0.88, respectively, with an overall autumn average of +0.60.

The Multivariate ENSO Index[5] (MEI), produced by the Physical Sciences Division of the Earth Systems Research Laboratory (formerly known as the US Climate Diagnostics Center), is derived from a number of atmospheric and oceanic parameters calculated as a two-month mean. As with 5VAR, large negative anomalies in the MEI are usually associated with La Niña and, conversely, large positive anomalies indicate El Niño. The February–March (–0.02), March–April (+0.15) and April–May (+0.93) MEI values (not shown) display an increasing trend, like the 5VAR values. The substantial increase between the last two bi-monthly MEI values is the second biggest jump on record at this time of year, second only to the return to neutral conditions in 2011 (Tobin and Skinner 2012). This reflects a strong push towards El Niño in most indicators.

### Outgoing long-wave radiation

Outgoing long-wave radiation (OLR) in the equatorial Pacific Ocean is a good proxy for tropical convection, with decreases (increases) in OLR associated with increased (decreased) convection, and thus cloudiness and rainfall. In particular, during El Niño decreased OLR, or increased convection, often occurs near the Date Line. The opposite is true during La Niña.

Standardised monthly anomalies[6] of OLR are computed for an equatorial region from 5°S to 5°N and 160°E to 160°W by NOAA's Climate Prediction Center. Monthly values for autumn were –1.1 for March, –1.0 for April and –0.1 for May, with an autumn average of –0.7. The negative values seen during March and April were most likely a result of increased cyclonic activity in the far western Pacific at the time.

The spatial pattern of seasonal OLR anomalies across the Asia–Pacific region between 40°S and 40°N are shown in Fig. 3. As mentioned above, increased cyclonic activity in the far western Pacific during March and April can be seen in the overall autumn map below, with negative OLR anomalies over much of the region. Likewise, negative OLR anomalies can be seen across much of southern Australia, coinciding with increased rainfall for the region (see rainfall section).

[2]ENSO 5VAR was developed by the Bureau of Meteorology and is described in Kuleshov et al. 2009. The principal component analysis and standardisation of this ENSO index is performed over the period 1950–1999.

[3]MSLP data obtained from www.bom.gov.au/climate/current/soihtm1.shtml.

[4]SST indices obtained from ftp://ftp.cpc.ncep.noaa.gov/wd52dg/data/indices/sstoi.indices

[5]Multivariate ENSO Index obtained from www.esrl.noaa.gov/psd/people/klaus.wolter/MEI/table.html. The MEI is a standardised anomaly index described in Wolter and Timlin 1993, and 1998.

[6]Obtained from www.cpc.ncep.noaa.gov/data/indices/olr

Fig. 3. OLR anomalies for autumn 2014 (W m$^{-2}$). Base period is 1979–2000.

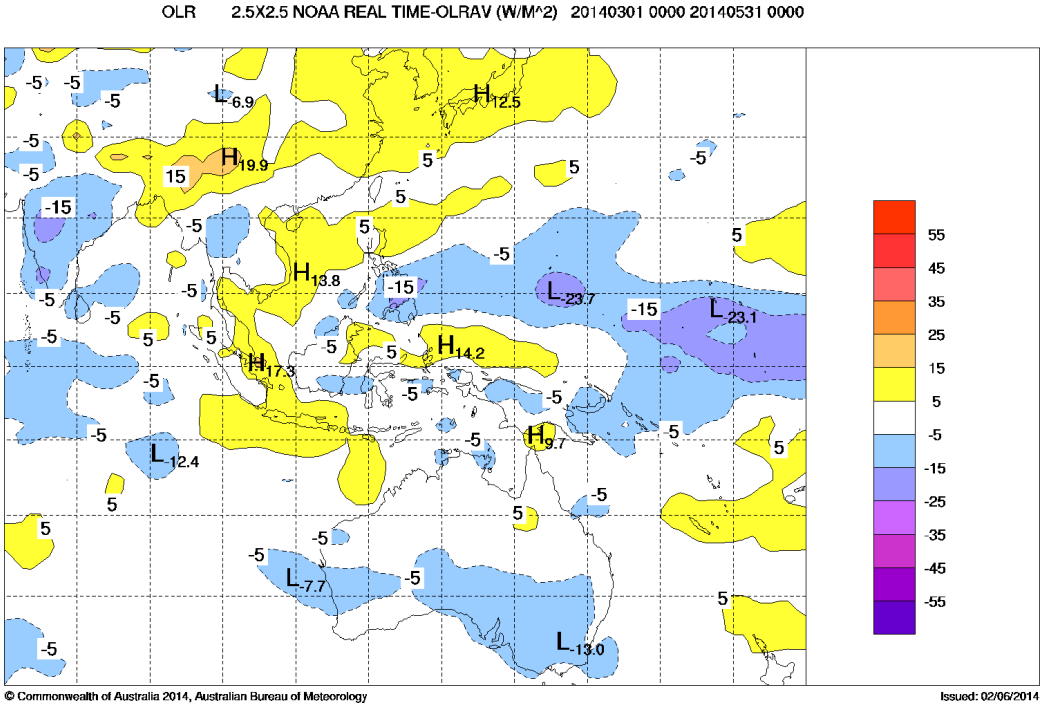


Fig. 4. Time-longitude section of daily-averaged OLR anomalies, averaged for 15°S to 15°N, for the period December 2013 to June 2014. Anomalies are with respect to a base period of 1979–2010.

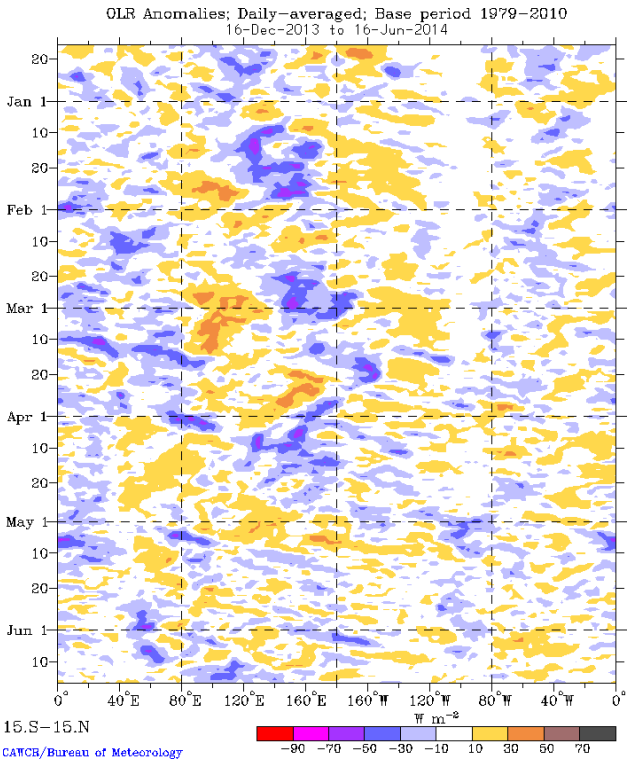


Over much of the Maritime Continent, OLR anomalies were fairly patchy. Through Asia OLR anomalies were generally positive, except over India, which had negative anomalies.

### Madden–Julian Oscillation

The Madden–Julian Oscillation (MJO) is a tropical atmospheric anomaly which develops in the Indian Ocean and propagates eastwards into the Pacific Ocean (Madden and Julian 1971, 1972, and 1994). The MJO takes approximately 30 to 60 days to reach the western Pacific, with a frequency of six to twelve events per year (Donald et al. 2004). When the MJO is in an active phase, it is associated with large scale convergence at the surface that results in areas of increased and decreased tropical convection. The effects of the MJO during autumn are transitioning from the southern to northern hemisphere. The MJO is monitored by the Real-time Multivariate MJO (RMM) index. A description of this index and the associated phases can be found in Wheeler and Hendon (2004).

The phase-space diagram of the RMM index for autumn is shown in Fig. 5, and the evolution of tropical convection anomalies along the equator with time is shown in Fig. 4. The period from March to May 2014 shows two weak pulses of MJO activity. The first MJO pulse occurred in late March to early April, originating in the western Indian Ocean (phase two). It progressed out to the Date Line (phase six), weakening in mid to late April. This pulse was the last one to affect the northern Australian 2013–14 wet season. The second MJO pulse occurred in early May, progressing across the African region (phase eight), and decaying in the far eastern Indian Ocean (phase three) in mid-May.

Fig. 5. Phase-space representation of the MJO index for austral autumn 2014. Daily values are shown with March in red, April in green, and May in blue.

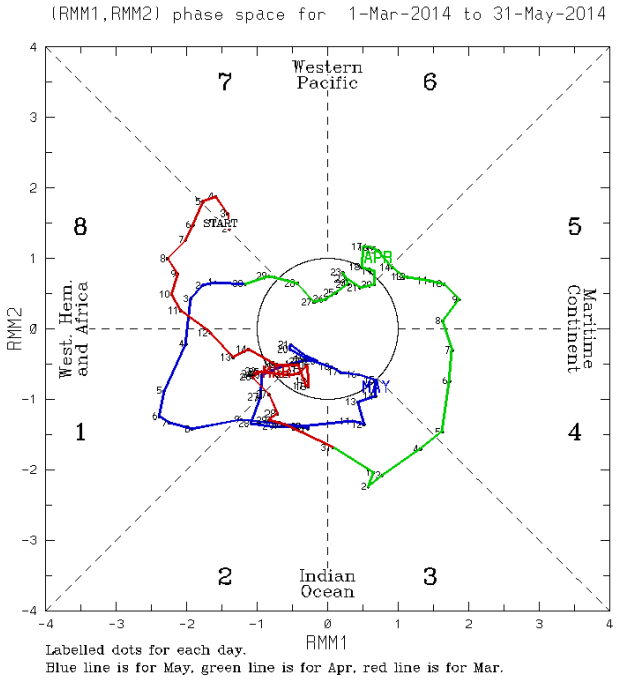


## Oceanic patterns

### Sea-surface temperatures

Autumn 2014 global sea-surface temperature (SST) anomalies, from the US National Oceanic and Atmospheric Administration (NOAA) Optimum Interpolation analyses (Reynolds et al. 2002) are displayed in Fig. 6. Positive (warm) anomalies are shown in red shades, while negative (cool) anomalies are shown in blue shades.

During summer, the SSTs across the tropical Pacific reflected that of a neutral ENSO state (Tihema 2014). In the eastern tropical Pacific, warm anomalies emerged during autumn, steadily increasing in magnitude through each autumn month; a pattern typical of El Niño development. In the eastern Pacific, the NINO3 index warmed significantly from –0.24 °C in March to +0.61 °C in May. Similarly in the central Pacific, NINO3.4 also warmed, from –0.22 °C in March to +0.46 °C in May.

Warm anomalies were also present during autumn in the western tropical Pacific Ocean and in the Indian Ocean south of the equator. These warm anomalies extended to cover much of the Australian region and Maritime Continent. Other notable anomalies across the southern hemisphere include a large pool of warmer than average water to the east of Argentina and warm anomalies across southern parts of the Pacific Ocean.

SSTs in the Australian region (described by a box from 0°S to 50°S and 94°E to 174°E), ranked as equal fourth warmest on record for autumn, behind 1998, 2010, and 2013.

### Equatorial Pacific sub-surface patterns

The time longitude (Hovmöller) diagram for the 20 °C isotherm depth anomaly along the equator for January 2012 to May 2014, obtained from the TAO Project Office[7], is shown in Fig. 7. The 20 °C isotherm depth is generally located close to the equatorial thermocline, which is the region of greatest temperature gradient with depth, and is the boundary between the warm near-surface and cold deep ocean waters. Therefore, measurements of the 20 °C isotherm make a good proxy for the thermocline depth. Positive (negative) anomalies correspond to the 20 °C isotherm being deeper (shallower) than average. A lowering (lifting) of the thermocline depth results in less (more) cold water available for upwelling, and therefore a warming (cooling) of surface temperatures.

The end of 2013 and early 2014 show notable changes in 20 °C isotherm depth. The eastward progression of two downwelling Kelvin waves warmed the subsurface, and lowered the 20 °C isotherm significantly. The first downwelling Kelvin wave was a fairly weak one, which reached the eastern Pacific near the end of December 2013 (seen by the eastward progression of positive anomalies), and the second was a strong one, reaching the east by the end of autumn 2014. The second Kelvin wave lowered the 20 °C isotherm by 30 to 40 metres in parts of the central to eastern Pacific. The rate of warming was in some respects similar to the development of the 1997–98 El Niño (for a summary, see Beard 1998).

Figure 8 shows a cross-section along the equator (2°S to 2°N) of monthly subsurface anomalies from February to May 2014 (obtained from the Bureau of Meteorology). Red shading indicates positive anomalies and blue shades indicate negative anomalies. The lowering of the 20 °C isotherm (as discussed above) and warming of the subsurface can be seen clearly here in the four-month plot, with the eastward progression of the strong Kelvin wave seen through the progression of warm anomalies towards the eastern Pacific surface.

## Atmospheric patterns

### Surface analyses

The mean sea level pressure (MSLP) pattern for autumn 2014 is shown in Fig. 9, computed using data from the 0000 UTC daily analyses of the Bureau of Meteorology's Australian Community Climate and Earth System Simulator (ACCESS) model[8]. The MSLP anomalies are shown in Fig. 10, relative to the 1979–2000 climatology obtained from the National Centers for Environmental Prediction (NCEP) II Reanalysis data (Kanamitsu et al. 2002). The MSLP anomaly field is not shown over areas of elevated topography (grey shading).

Showing a weak three-wave structure, the autumn 2014 mean MSLP was zonal in the mid to high latitudes,

[7]Hovmöller plot obtained from www.pmel.noaa.gov/tao/jsdisplay
[8]For more information on the Bureau of Meteorology's ACCESS model, see www.bom.gov.au/nwp/doc/access/NWPData.shtml

Fig. 6. Anomalies of global SST for austral autumn 2014 (°C).

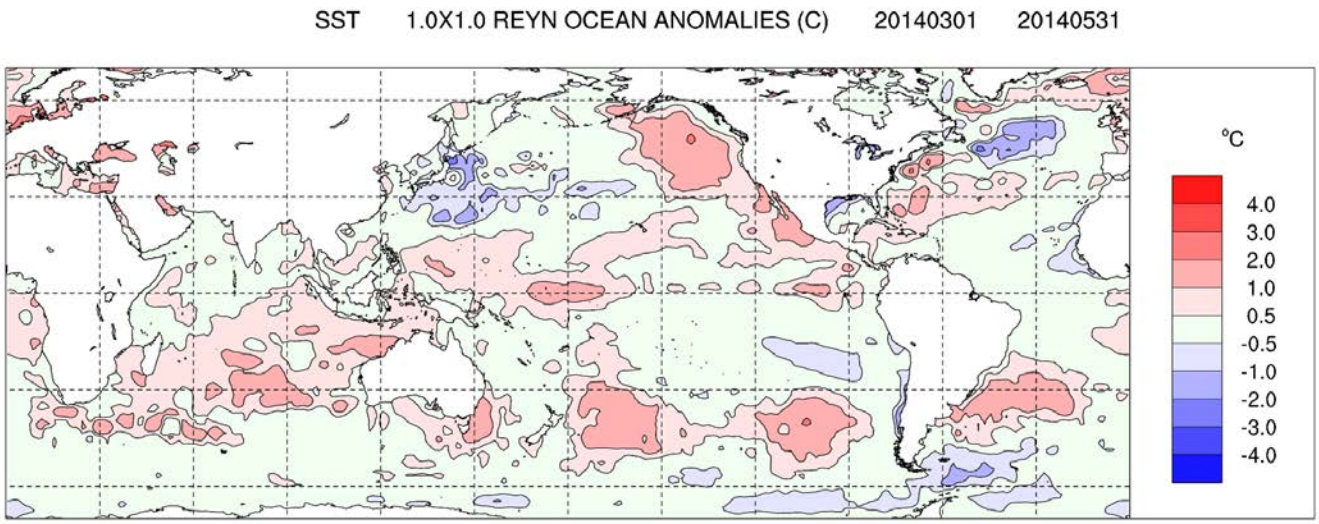


Fig. 7. Time-longitude section of the monthly anomalous depth of the 20 °C isotherm at the equator (2°S to 2°N) for January 2012 to May 2014. (Plot obtained from the TAO Project Office).

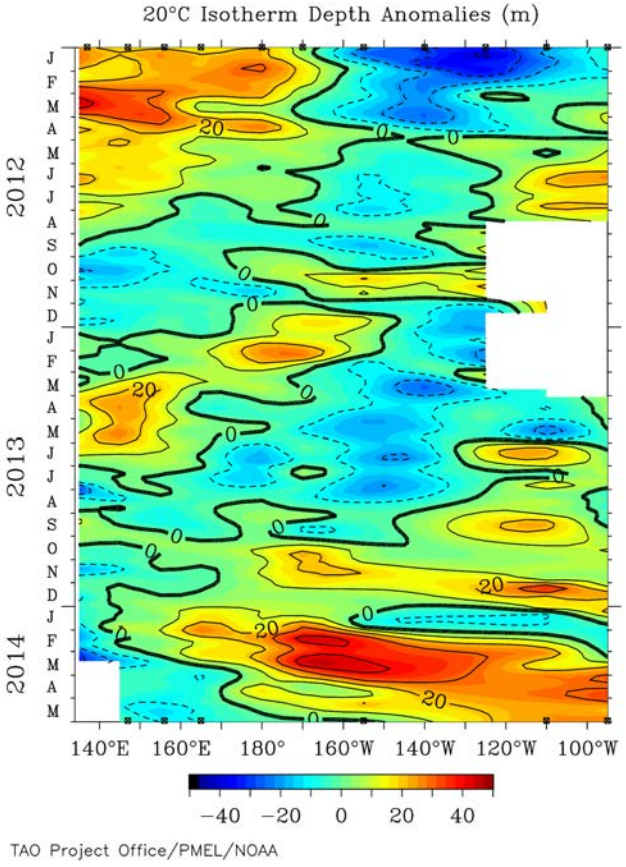


Fig. 8. Four-month sequence from February to May 2014 of vertical sea subsurface temperature anomalies at the equator for the Pacific Ocean. The contour interval is 0.5 °C. (Plot obtained from the Bureau of Meteorology*).

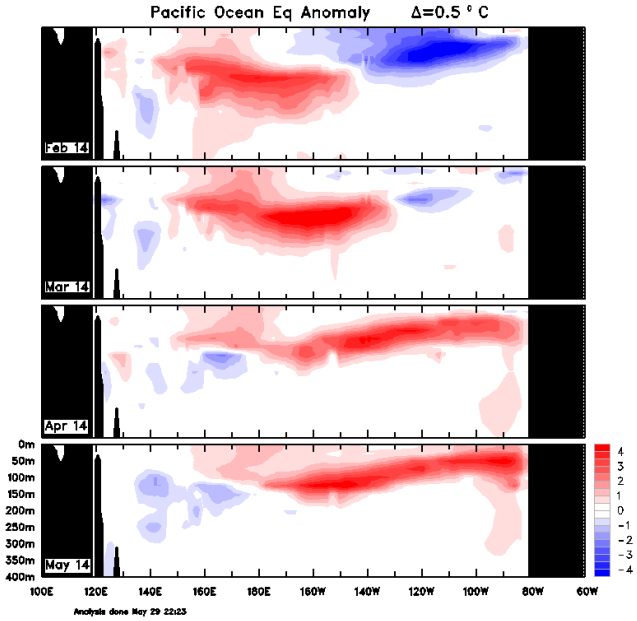


*This and other analyses available from www.bom.gov.au/oceanography/oceantemp/pastanal.shtml

Fig. 9. Autumn 2014 MSLP (hPa). The contour interval is 5 hPa.

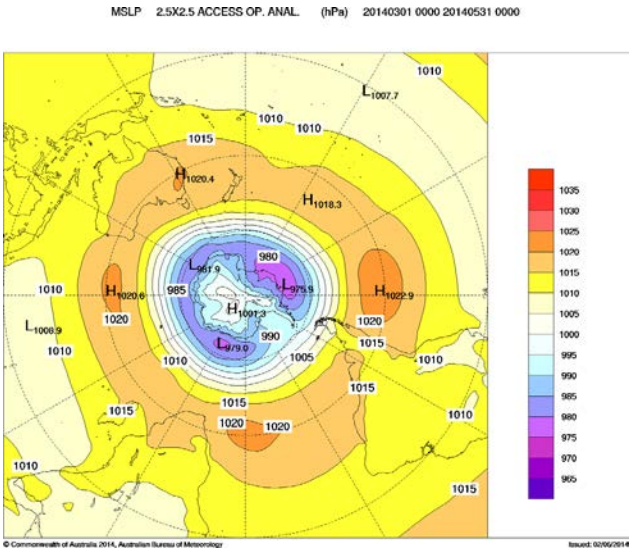


Fig. 10. Autumn 2014 MSLP anomalies (hPa), from a 1979–2000 climatology.

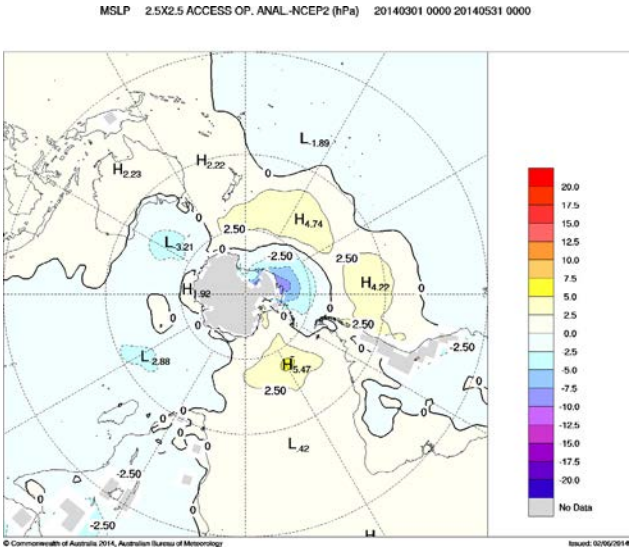


Fig. 11. Autumn 2014 500 hPa mean geopotential height (gpm).

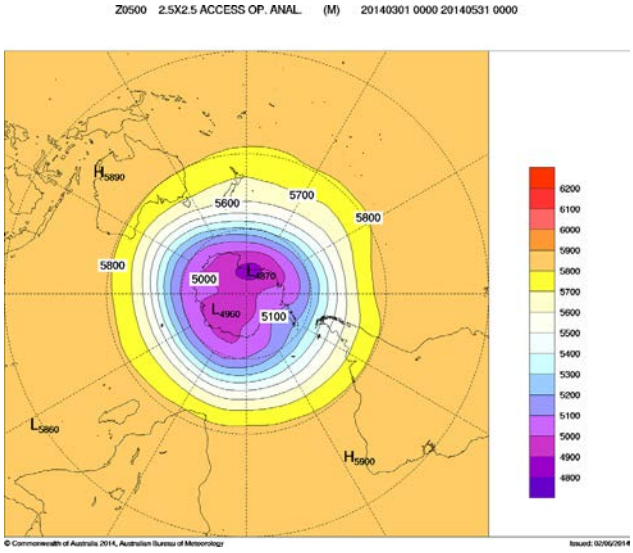


Fig. 12. Autumn 2014 500 hPa mean geopotential height anomalies (gpm), from a 1979–2000 climatology.

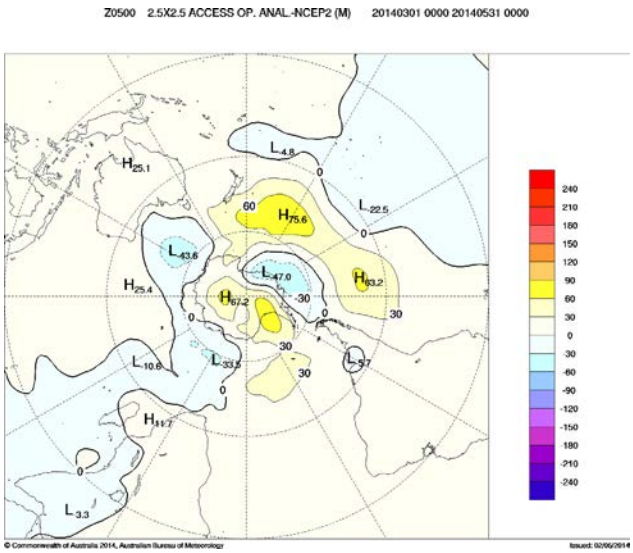


with troughs located at approximately 20°E, 120°E, and 120°W. The three-wave pattern is the most stable pattern for the atmosphere, and trough locations show the areas where low pressure was most favoured during autumn. The highest pressure for the season was located to the west of Chile in the Pacific Ocean (1022.9 hPa), with the lowest pressure to the south of it, just west of the Antarctic Peninsula (975.9 hPa).

Notable areas of anomalous high pressure were recorded across the southern Pacific Ocean, with anomalies of almost +5 hPa, and to the east of Argentina in the southern Atlantic Ocean, just exceeding +5 hPa. Anomalous low pressure was present to the west of the Antarctic Peninsula. This MSLP anomaly pattern has some similarities to the loading pattern for the positive phase of the Southern Annular Mode (SAM), which is discussed in more detail in a following section.

### Mid-tropospheric analyses

The 500 hPa geopotential height is a good indicator of the steering of surface synoptic systems across the southern hemisphere. The mean for autumn 2014 is shown in Fig. 11, with the associated anomalies in Fig. 12. The autumn 500 hPa height pattern in Fig. 11 shows the characteristic zonal structure in the mid to high latitudes, with weak three-wave characteristics that were also noted in Fig. 9 for the mean MSLP pattern. The 500 hPa anomaly pattern is similar to that at the surface (Fig. 10).

Fig. 13. Austral autumn 2014 850 hPa vector wind anomalies (m s$^{-1}$).

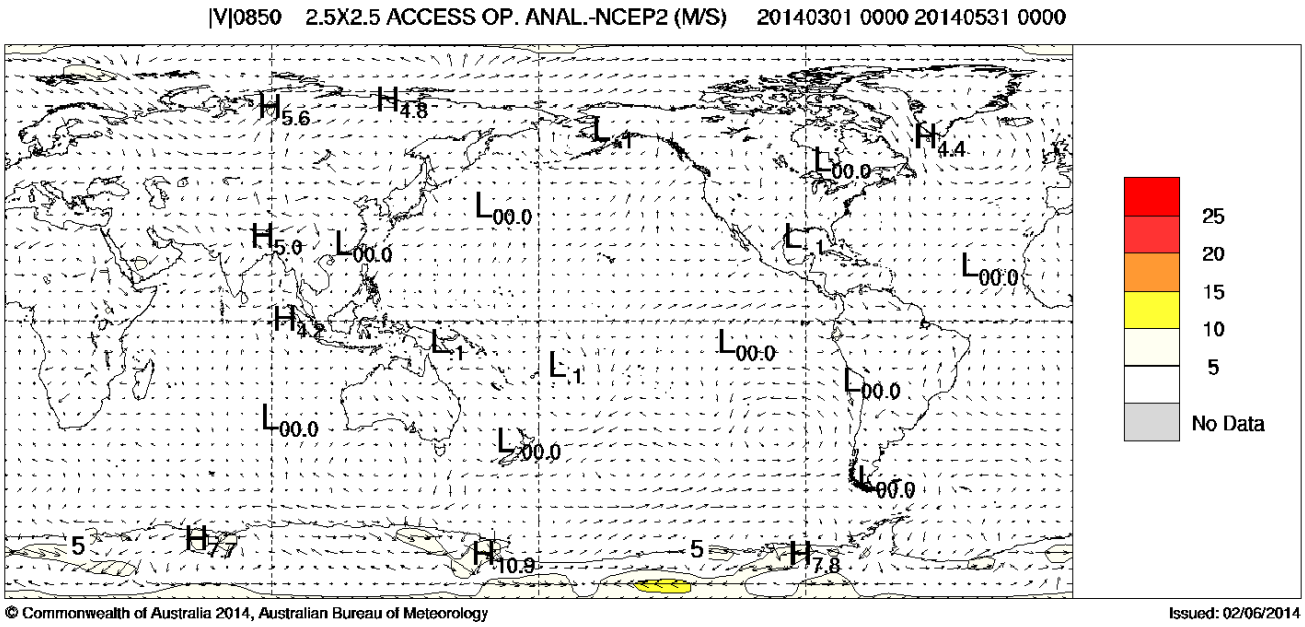


### Southern Annular Mode

The Southern Annular Mode (SAM) describes the periodic, approximately ten day oscillation of atmospheric pressure between the polar and mid-latitude regions of the southern hemisphere. Positive phases are characterised by mass shifting towards the mid-latitudes, and away from the poles (meaning anomalous high pressure in the mid-latitudes, and thus a poleward shift in the mid-latitude westerly jet). Conversely, negative phases are characterised by mass shifting towards Antarctica (meaning anomalous low pressure in the mid-latitudes, and an equatorward shift in the jet). A similar oscillation exists in the northern hemisphere, the Northern Annular Mode, or NAM.

The Climate Prediction Center[9] produces a standardised monthly SAM index. The March, April and May values were +0.47, +0.61 and –0.45, respectively, with an overall autumn value slightly positive at +0.21. As mentioned earlier, the autumn MSLP anomaly pattern (Fig. 10) shares some similarities to the loading pattern for the positive SAM phase, with anomalous low pressure closer to Antarctica, and anomalous high pressure further north around the 40°S–50°S band. At this time of year, the SAM impact on Australian rainfall is generally weak (see Hendon et al., 2007).

### Winds

Austral autumn 2014 low-level (850 hPa) and upper-level (200 hPa) wind anomalies (as per the surface analyses, computed from ACCESS and anomalies with respect to the 22-year NCEP II climatology) are shown in Figs 13 and 14, respectively. Isotach contours are at 5 m s$^{-1}$ intervals.

Low-level 850 hPa anomalies for the autumn season were generally within 5 m/s of the long-term average. Over Australia, weak northwesterly low-level wind anomalies can be seen feeding across the Kimberley in Western Australia, down towards South Australia and Victoria. The weak westerly anomaly in the central to eastern Pacific Ocean near the equator helps explain the increase in sea surface temperatures across the region during the autumn months (see Oceanic patterns section).

Upper-level 200 hPa anomalies show westerly winds across much of the 40°S–50°S band (except to the south of Australia), consistent with a southward shift in the polar-front jet, and likewise consistent with weakly positive SAM.

## Australian region

### Rainfall

Australian rainfall totals for autumn 2014 are shown in Fig. 15, with corresponding rainfall deciles shown in Fig. 16. The deciles are calculated using gridded rainfall data for all autumn periods between 1900 and 2014. Autumn rainfall for Australia was slightly below normal, with an area-average of 109.8 mm, nine per cent below the 1961–90 average. However, given the high skewness of Australian rainfall, autumn 2014 rainfall was slightly above median, ranking 61st out of 115 years (see Table 1).

Notable areas of above average rainfall were generally located across the southern regions, with totals in the top 30 per cent of autumn records measured in an area extending from eastern Western Australia, through South Australia and parts of central Australia, and across to eastern parts of New South Wales and northern Victoria. Parts of this

[9]Climate Prediction Center (NOAA) monthly mean Antarctic Oscillation (AAO, or SAM) index since January 1979 http://www.cpc.ncep.noaa.gov/products/precip/CWlink/daily_ao_index/aao/aao.shtml

Fig. 14. Austral autumn 2014 200 hPa vector wind anomalies (m $s^{-1}$).

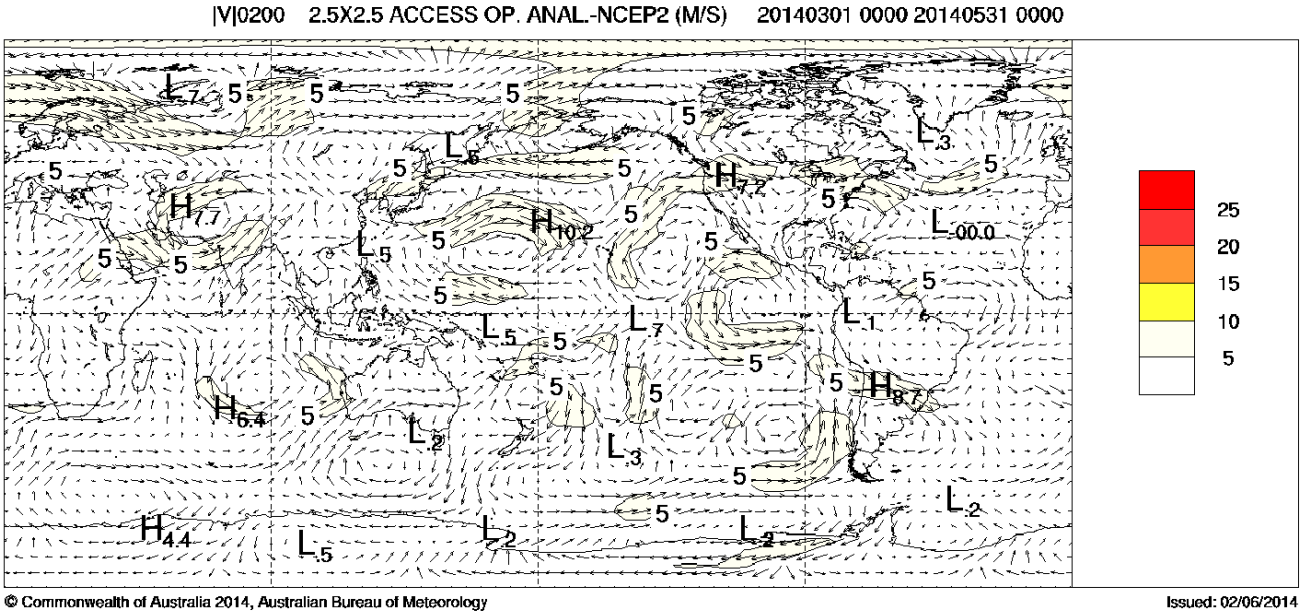


Fig. 15. Autumn 2014 rainfall totals (mm) for Australia.

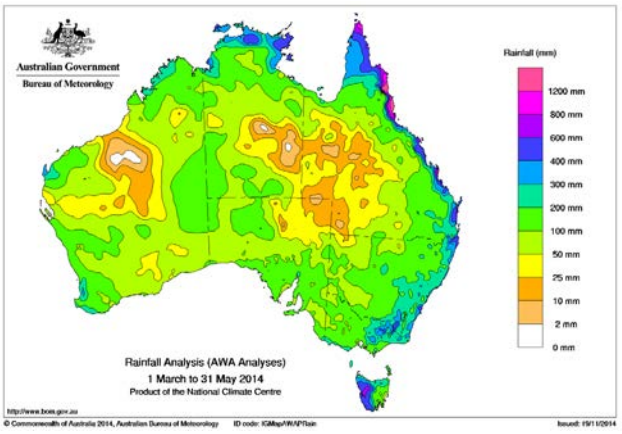


Fig. 16. Autumn 2014 rainfall deciles for Australia: decile ranges based on grid-point values over all autumns from 1900 to 2014.

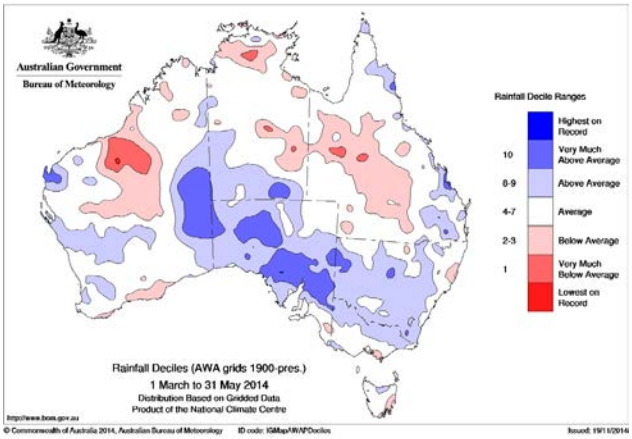


Fig. 17. Rainfall deficiencies for the 22-month period 1 August 2012 to 31 May 2014.

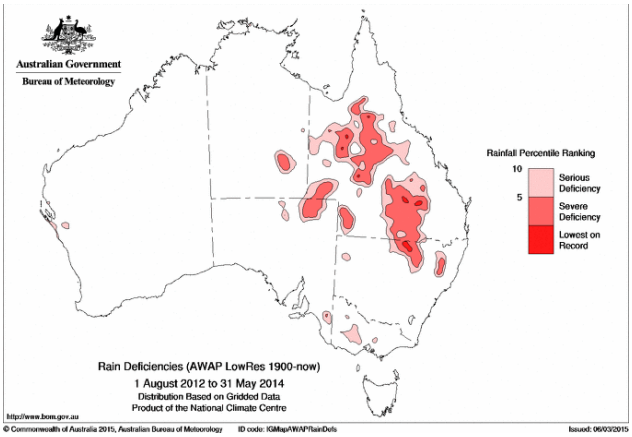


Fig. 18. Autumn 2014 maximum temperature anomalies (°C).

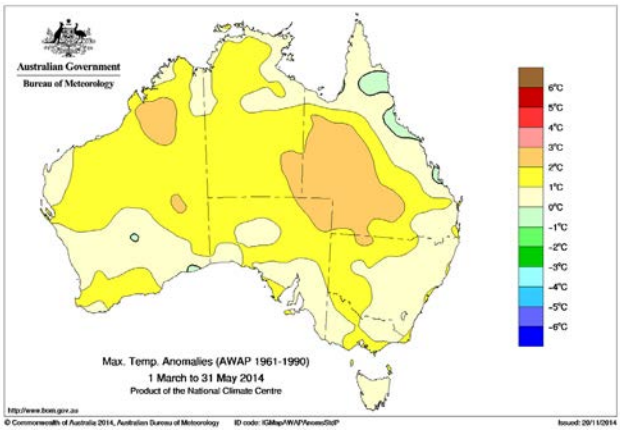

area experienced rainfall in the highest ten per cent of totals, mostly in South Australia. This contributed to South Australia being the only State to record rainfall in their top (or bottom) 20 years, ranking 13th wettest of 115 years (see Table 1). Other smaller notable areas with above average rainfall were located across the Queensland east coast, and across parts of Western Australia. An area surrounding Exmouth had localised high autumn rainfall totals—this was a result of two heavy rainfall events, one of which was ex-tropical cyclone *Jack* combining with a mid-level trough.

Aside from South Australia, statewide average rainfall in New South Wales and Victoria was also above average, while the remaining States were below average. However, none had notable deviations from average, with all of them within 25 per cent of the long-term mean. On a smaller scale, areas of below average rainfall (bottom 30 per cent of historical totals) were recorded across western Queensland, parts of the Pilbara and Gascoyne Districts in Western Australia, and across the Northern Territory's Top End.

Four cyclones occurred in the Australian region during

Fig. 19. Autumn 2014 maximum temperature deciles: decile ranges based on grid-point values for all autumns from 1911 to 2014.

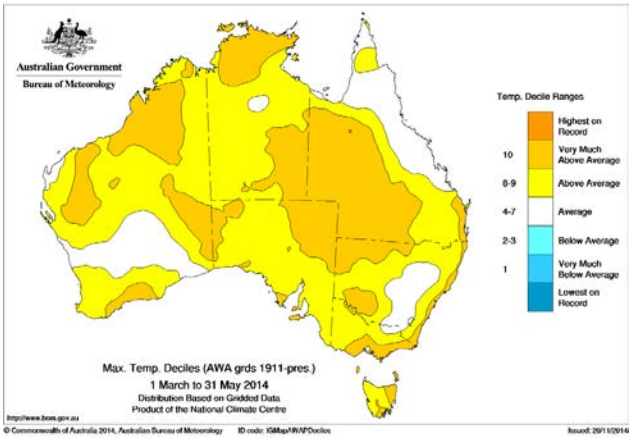


Fig. 20. Autumn 2014 minimum temperature anomalies (°C).

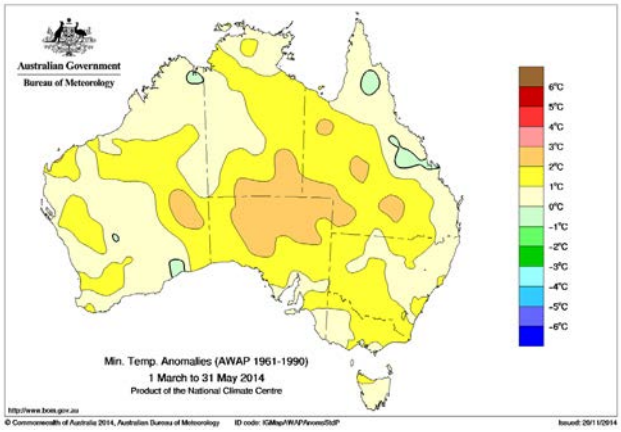


Table 1. Summary of the seasonal rainfall ranks and extremes on a national and State basis for autumn 2014. The ranking in the second-last column goes from 1 (lowest) to 115 (highest) and is calculated over the years 1900 to 2014 inclusive.

| *Region* | *Highest seasonal total (mm)* | *Lowest seasonal total (mm)* | *Highest daily total (mm)* | *Area-averaged rainfall (mm)* | *Rank of area-averaged rainfall* | *Per cent difference from mean* |
|---|---|---|---|---|---|---|
| Australia | 3895.6 at Bellenden Ker Top Station (Qld) | Zero at several locations | 450.7 at Numinbah State Farm (Qld) on 28 March | 109.7 | 61 | –9% |
| Queensland | 3895.6 at Bellenden Ker Top Station | Zero at several locations | 450.7 at Numinbah State Farm on 28 March | 127.8 | 50 | –22% |
| New South Wales | 648.2 at Yarras (Mt Seaview) | 16.4 at Innamincka Hotel | 317.0 at Boat Harbour (Rous River) on 28 March | 151.7 | 89 | +6% |
| Victoria | 572.8 at Mt Hotham | 64.2 at Telangatuk East | 93.4 at Mt Nowa Nowa on 12 April | 171.5 | 84 | +9% |
| Tasmania | 933.2 at Mt Read | 62.0 at Grindstone Point | 70.2 at Mt Victoria on 22 April | 318.5 | 49 | –7% |
| South Australia | 239.8 at Belair | 16.4 at Innamincka Hotel | 126.0 at Wirraminna Homestead on 10 April | 87.6 | 104 | +56% |
| Western Australia | 401.8 at Learmonth Airport | 0.6 at Telfer Aero | 206.0 at Exmouth Town on 27 April | 82.2 | 53 | –9% |
| Northern Territory | 552.2 at Gove Airport | Zero at several locations | 150.0 at Gorrie on 03 March | 107.6 | 52 | –23% |

Table 2. Summary of the seasonal maximum temperature ranks and extremes on a national and State basis for autumn 2014. The ranking in the last column goes from 1 (lowest) to 105 (highest) and is calculated over the years 1910 to 2014 inclusive.

| *Region* | *Highest seasonal mean maximum (°C)* | *Lowest seasonal mean maximum (°C)* | *Highest daily temperature (°C)* | *Lowest daily maximum temperature (°C)* | *Area-averaged temperature anomaly (°C)* | *Rank of area-averaged temperature anomaly* |
|---|---|---|---|---|---|---|
| Australia | 37.4 at Fitzroy Crossing (WA) | 8.6 at Mt Hotham (Vic) | 44.6 at Roebourne (WA) on 7 March | -1.2 at Charlotte Pass (NSW) and Thredbo (NSW), both on 2 May | +1.16 | 100 |
| Queensland | 35.6 at Julia Creek Airport | 21.8 at Applethorpe | 42.1 at Birdsville Airport on 15 March | 9.5 at Applethorpe on 4 May | +1.21 | 95 |
| New South Wales | 29.2 at Wanaaring | 9.3 at Thredbo | 39.1 at Pooncarie on 10 March | -1.2 at Charlotte Pass and Thredbo both on 2 May | +0.94 | 95 |
| Victoria | 24.9 at Mildura | 8.6 at Mt Hotham | 38.4 at Ouyen on 10 March | -1.0 at Mt Hotham on 2 May | +0.89 | 95 |
| Tasmania | 19.9 at Flinders Island | 9.0 at Mt Wellington | 33.2 at Swansea on 11 March | 0.0 at Mt Wellington on 6 May | +0.71 | 95 |
| South Australia | 30.7 at Moomba | 17.7 at Mt Lofty | 41.0 at Marree on 10 March | 7.7 at Mt Lofty on 2 May | +1.29 | 95 |
| Western Australia | 37.4 at Fitzroy Crossing | 21.0 at Albany | 44.6 at Roebourne on 7 March | 13.5 at Mount Barker on 1 May | +1.13 | 98 |
| Northern Territory | 36.8 at Bradshaw | 28.9 at Arltunga | 40.9 at Alice Springs on 15 March | 15.8 at Arltunga on 30 April | +1.27 | 95 |

Table 3. Summary of the seasonal minimum temperature ranks and extremes on a national and State basis for autumn 2014. The ranking in the last column goes from 1 (lowest) to 105 (highest) and is calculated over the years 1910 to 2014 inclusive.

| *Region* | *Highest seasonal mean minimum (°C)* | *Lowest seasonal mean minimum (°C)* | *Highest daily minimum temperature (°C)* | *Lowest daily temperature (°C)* | *Area-averaged temperature anomaly (°C)* | *Rank of area-averaged temperature anomaly* |
|---|---|---|---|---|---|---|
| Australia | 26.8 at Troughton Island (WA) | 2.6 at Thredbo (NSW) | 31.0 at Karratha (WA) on 13 March | -9.4 at Perisher Valley (NSW) on 8 May | +1.14 | 103 |
| Queensland | 25.6 at Coconut Island | 10.2 at Applethorpe | 28.6 at Bedourie on 8 April | -2.0 at Stanthorpe and at Applethorpe on 6 May | +1.31 | 101 |
| New South Wales | 18.4 at Byron Bay | 2.6 at Thredbo | 25.0 at White Cliffs on 12 March | -9.4 at Perisher Valley on 8 May | +1.24 | 100 |
| Victoria | 14.3 at Wilsons Promontory | 3.3 at Mt Hotham | 24.6 at Walpeup on 11 March | -4.9 at Mt Hotham on 7 May | +1.23 | 101 |
| Tasmania | 13.2 at Swan Island | 2.8 at Mt Wellington | 19.6 at Flinders Island on 2 April and 5 March | -7.4 at Liawenee on 8 May | +0.72 | =89 |
| South Australia | 17.0 at Moomba | 9.1 at Padthaway South | 27.9 at Oodnadatta on 15 March | -1.3 at Coonawarra on 8 May and at Naracoorte on 27 April | +1.86 | 105 |
| Western Australia | 26.8 at Troughton Island | 9.9 at Jarrahwood | 31.0 at Karratha on 13 March | 0.3 at Wandering on 2 May | +0.81 | =93 |
| Northern Territory | 26.5 at Cape Don | 14.0 at Arltunga | 29.2 at Mccluer Island on 1 April | 4.3 at Yulara on 31 May | +0.95 | 92 |

autumn: *Hadi, Gillian, Ita* and *Jack*. *Hadi* was located off the east coast of Australia, but did not make landfall. Likewise, during its time as a tropical cyclone, *Jack* remained in the Indian Ocean to the west of Western Australia (although as discussed above its remnants went on to affect Exmouth). Tropical cyclone *Gillian* was an exceptionally long-lived tropical low (organised and identifiable for 20 days), affecting the waters of Queensland, the Northern Territory and Western Australia. It was relatively weak in its first two weeks as a system around the Gulf of Carpentaria, but when it moved westwards out into the Indian Ocean, it briefly reached category 5 status. Tropical cyclone *Ita* formed as a tropical low to the southwest of the Solomon Islands at the start of April, and slowly intensified as it drifted westwards. On 10 April, *Ita* rapidly intensified to category 4, and then category 5 in approximately six hours, and turned southwestwards towards the far north Queensland coast. It made landfall near Cape Flattery on 11 April as a category 4 cyclone. It then rapidly weakened, and progressed along the Queensland coastline, shifting back out to sea near Proserpine on 13 April as a category 1 cyclone. *Ita* caused significant damage to sugarcane and banana plantations, with an estimation of about 90 per cent of sugarcane crops in the region wiped out by the storm.

### Drought

As discussed in the previous section, rainfall was below average across much of western Queensland, a relatively persistent feature over approximately the past two years. A way in which the Bureau of Meteorology assesses drought is by considering the extent of areas of the country which contain accumulated rainfall in the lowest ten per cent of records for varying time scales. To the end of May 2014, local temporal maxima in the areal extent of rainfall deficiencies occurred at periods of 22, 38 and 50 months.

For the 22-month period August 2012 to May 2014 (Fig. 17), 12.1 per cent of Australia was experiencing at least serious rainfall deficiencies (lowest ten per cent of records), with 5.8 per cent experiencing severe deficiencies (lowest five per cent of records). Most of this area was confined to western Queensland and adjacent interstate areas.

For the 38-month and 50-month periods (not shown), less than three per cent of Australia had recorded rainfall in the lowest ten per cent of records, with the 38-month period affecting small isolated areas of central Australia and western Victoria (this contributed to 23.7 per cent of Victoria experiencing serious rainfall deficiencies for the 38-month period), and the 50-month period affecting southwest Western Australia.

### Temperature

Australian maximum and minimum temperature anomalies are shown in Figs 18 and 20. Seasonal anomalies are calculated with respect to the 1961–1990 period, and use all stations for which an elevation is available (for details and for more information on the gridded dataset see Jones et al. (2009)). Station normals have been estimated using gridded climatologies for those stations with insufficient data within the 1961–1990 period to calculate a station normal directly. Figures 19 and 21 show maximum and minimum temperature deciles, calculated using gridded temperature data for all autumn periods between 1910 and 2014.

Mean maximum temperatures for autumn were above average over most of Australia, with the main exception being parts of Queensland's east coast. Anomalies in excess of +2.0 °C were recorded across a large area of western Queensland and areas extending into adjacent States. Other smaller areas exceeding +2.0 °C were recorded in Western Australia, with one in the Kimberley to the east of Broome, and another smaller area to the west of Giles. Considerable areas experienced maximum temperatures in the highest decile (37 per cent of Australia), including: the Northern Territory's Top End; large parts of Western Australia; much of western Queensland extending into adjacent States; and along the coastline in southeast Queensland, New South Wales, Victoria and eastern Tasmania. For statewide averages, Western Australia had its eighth warmest autumn, while the other States finished outside the top ten. Overall, the Australian area average came in at +1.16 °C for autumn, ranking sixth warmest of 105 years. See Table 2 for a full summary.

There was an exceptional heatwave experienced during May (Bureau of Meteorology 2014) which contributed towards the autumn warmth across much of the country. Warm sea surface temperatures to the east of Australia during May (not shown) may have limited the cooling effect of the sea breeze on maximum temperatures in coastal areas; this would in part explain the autumn decile pattern seen in Fig. 19, with decile 10 along much of the southeastern coastline.

Like maximum temperatures, minimum temperatures for autumn were warmer than average across most of Australia, except for a few small areas in the northeast of the country, and a few small isolated areas in Western Australia. The highest anomalies for autumn were +2 °C to +3 °C, which were measured across broad areas of central Australia. In terms of deciles, autumn minimum temperatures were in the highest decile across large areas of Australia (see Fig. 21). Overall, decile 10 covered 53 per cent of Australia. Parts of central Australia measured their warmest autumn nights on record. With significant areas of all States in decile 10, autumn nights were amongst the top ten records for most States (except Western Australia and the Northern Territory). South Australia as a whole was warmest on record, Queensland and Victoria fifth warmest, New South Wales sixth warmest, and Tasmania equal seventh warmest, with Australia as a whole ranked third warmest of 105 autumns for night-time temperatures (Table 3).

Fig. 21. Autumn 2014 minimum temperature deciles: decile ranges based on grid-point values for all autumns from 1911 to 2014.

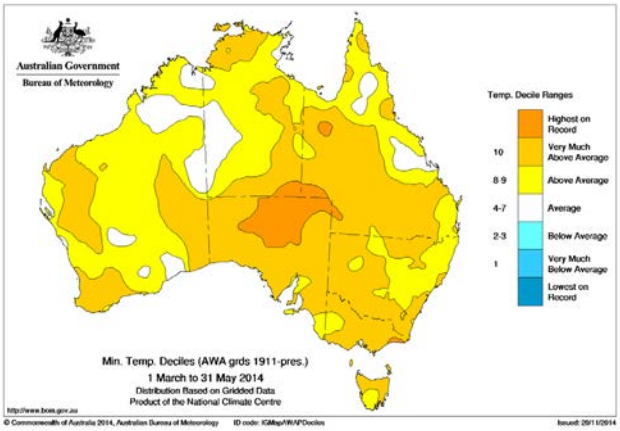


## References


Beard, G. 1998. Seasonal climate summary southern hemisphere (autumn 1997): rapid onset of a negative phase of the Southern Oscillation (El Niño). *Aust. Met. Mag., 47,* 55–62.

Bureau of Meteorology, 2014. An exceptionally prolonged autumn warm spell over much of Australia. *Special Climate Statement 49*. Bureau of Meteorology, Melbourne, Australia. www.bom.gov.au/climate/current/special-statements.shtml

Campbell, B. 2011. Seasonal climate summary southern hemisphere (autumn 2010): rapid decay of El Niño, wetter than average in central, northern and eastern Australia and warmer than usual in the west and south. *Aust. Met. Oceanogr. J., 61,* 65–76.

Cottrill, D.A. 2012. Seasonal climate summary southern hemisphere (spring 2011): La Niña returns. *Aust. Met. Oceanogr. J., 62,* 179–192.

Donald, A., Meinke, H., Power, B., Wheeler, M. and Ribbe, J. 2004. Forecasting with the Madden-Julian Oscillation and the applications for risk management. 4th International Crop Science Congress, 26 September – 1 October 2004, Brisbane, Australia.

Ganter, C. 2011. Seasonal climate summary southern hemisphere (winter 2010): a fast developing La Niña. *Aust. Met. Oceanogr. J., 61,* 125–135.

Hendon, H.H., Thompson, D.W.J., and Wheeler, M.C. 2007. Australian rainfall and surface temperature variations associated with the southern hemisphere annular mode. *J. Clim., 20,* 2452–2467.

Jones, D.A., Wang, W. and Fawcett, R. 2009. High-quality spatial climate data-sets for Australia. *Aust. Met. Oceanogr. J., 58,* 233–248.

Kanamitsu, M., Ebisuzaki, W., Woollen, J., Yang, S.-K, Hnilo, J.J., Fiorino, M. and Potter, G.L. 2002. NCEP-DOE AMIP-II Reanalysis (R-2). *Bull. Am. Meteorol. Soc., 83,* 1631–43.

Kuleshov, Y. Qi, L., Fawcett, R., Jones, D. 2009. 'Improving preparedness to natural hazards: Tropical cyclone prediction for the Southern Hemisphere,' in: Gan, J. (Ed.), *Advances in Geosciences, Vol. 12 Ocean Science*, World Scientific Publishing, Singapore, 127–43.

Madden, R.A., and Julian, P.R. 1971. Detection of a 40-50 day oscillation in the zonal wind in the tropical Pacific. *J. Atmos. Sci., 28,* 702–708.

Madden, R.A., and Julian, P.R. 1972. Description of global-scale circulation cells in the tropics with a 40-50 day period. *J. Atmos. Sci., 29,* 1109–1123.

Madden, R.A., and Julian, P.R. 1994. Observations of the 40-50 day tropical oscillation: a review. *Mon. Wea. Rev., 122,* 814–837.

Pepler, A. 2013. Seasonal climate summary southern hemisphere (winter 2012): dry conditions return to Australia. *Aust. Met. Oceanogr. J., 63,* 339–349.

Reynolds, R.W., Rayner, N.A., Smith, T.M., Stokes, D.C. and Wang, W. 2002. An improved in situ and satellite SST analysis for climate. *J. Clim., 15,* 1609–25.

Tihema, T. 2014. Seasonal climate summary southern hemisphere (summer 2013–14): warmer than average summer; neutral ENSO. *Aust. Met. Oceanogr. J., 64,* 331–344.

Tobin, S. 2012. Seasonal climate summary southern hemisphere (winter 2011): a dry season in the lull between La Niña events. *Aust. Met. Oceanogr. J.,* 62, 97–110.

Tobin, S., and Skinner, T.C.L. 2012. Seasonal climate summary southern hemisphere (autumn 2011): one of the strongest La Niña events on record begins to decline. *Aust. Met. Oceanogr. J., 62,* 39–50.

Troup, A.J. 1965. The Southern Oscillation. *Q. J. R. Meteor. Soc., 91,* 490–506.

Wheeler, M.C., and Hendon H.H. 2004. An All-Season Real-Time Multivariate MJO Index: Development of an Index for Monitoring and Prediction. *Mon. Weather Rev., 132,* 1917–32.

Wolter, K. and Timlin, M.S. 1993. Monitoring ENSO in COADS with a seasonally adjusted principal component index. *Proc. Of the 17th Climate Diagnostics Workshop,* Norman, OK, NOAA/NMC/CAC, NSSL, Oklahoma Clim. Survey, CIMMS and the School of Meteorology, Univ. of Oklahoma, 52–7.

Wolter, K. and Timlin, M.S. 1998. Measuring the strength of ENSO – how does 1997/98 rank? *Weather, 53,* 315–24.